JOURNAL OF THE KOREAN ASTRONOMICAL SOCIETY
33: 57 ~ 73, 2000

NONTHERMAL BROADENING OF UV LINES OBSERVED AT THE LIMB OF THE QUIET SUN

HYUNSOOK LEE[1], HONG SIK YUN[1], AND JONGCHUL CHAE[2]
[1]Astronomy program, School of Earth and Environmental Sciences, Seoul National University, Seoul 151-742, Korea
[2] Big Bear Solar Observatory, California, USA
E-mail: hslee@astro.snu.ac.kr, yun@astrosun.snu.ac.kr, and chae@bbso.njit.edu
(Received Jan. 15, 2000; Accepted Jan. 24, 2000)

ABSTRACT

We have done a spectroscopic study of the solar transition region using high resolution UV & EUV data obtained by SUMER(Solar Ultraviolet Measurements of Emitted Radiation) on board SOHO(Solar and Heliospheric Observatory). Optically thin and conspicuous emission lines observed at the solar limb are carefully selected to acquire average values of physical parameters for the quiet region as a function of radial distance.

Our main results found from the present study can be summarized as follows. 1) Nonthermal velocities estimated from various UV lines do not decrease with height at least within one total line intensity scale height above the limb. 2) Nonthermal velocity distribution with temperature is very similar to that of the disk center, in the sense that its peak is located around $2 \times 10^5 K$, but the value is systematically larger than that of the disk. 3) It is found that nonthermal velocity is inversely proportional to quadratic root of electron density up to about 10 arc seconds above the limb, i.e. $\xi \sim {N_e}^{-1/4}$, implying that the observed nonthermal broadening can be attributed to Alfvén waves passing through the medium. 4) Electron density estimated from the O V 629/760 line ratio is found to range from about $1 \times 10^{10} cm^{-3}$ to $2 \times 10^{12} cm^{-3}$ in the transition region.

Key words : Sun : transition region – SUN : UV – Spectroscophy : SUMER – Nonthermal velocity

I. INTRODUCTION

Nonthermal broadening of solar UV & EUV emission lines has been investigated by numerous workers(*e.g.*, Bruner et al. , 1973; Boland et al. , 1973; Boland et al. , 1975; Feldman, Doschek, & Tousey, 1975; Feldman, Doschek, & Patterson, 1976; Doschek et al. , 1976; Mariska, Feldman, & Doschek, 1978; Bruner & McWhirter, 1979; Dere et al. , 1987; Hassler et al. , 1990; Dere & Mason, 1993; Doyle et al. , 1997). They have demonstrated that there exists nonthermal kinetic energy component in the transition region between the upper chromosphere and the lower corona. The physical origin of this excessive broadening, however, still remains controversial.

Nonthermal motion is a local mass motion. Under collisional ionization equilibrium, i.e. $T_e = T_i$, the nonthermal velocity is estimated from the FWHM(Full Width Half Maximum) of an emission line profile after removing thermal contribution. In general, UV & EUV lines are optically thin and are well represented by Gaussian profiles.

The nonthermal velocity has been measured as a function of temperature in the solar atmosphere. Boland et al. (1975) showed that nonthermal velocity component increases with ionization temperature in the range of 6×10^3K to 10^5K. This tendency has been confirmed by Doyle et al. (1997) who worked with HRTS data and by Chae, Schühle, & Lemaire(1998) who dealt with SUMER(Solar Ultraviolet Measurements of Emitted Radiation) on board SOHO(Solar and Heliospheric Observatory). However, no conclusive evidence can be drawn on its temperature dependence above 2×10^5K, until Chae, Schühle, & Lemaire(1998) found that it gradually decreases with temperature.

Before launching SUMER, no UV & EUV spectrometer could observe the solar atmosphere with spatial resolution better than 1 arcsec and spectral resolution better than 50mÅ. One of early observations made by Shine et al. (1976) demonstrated that UV spectral lines off the limb were broader than those on the disk center. Nicolas et al. (1977) and Mariska, Feldman, & Doschek(1978) showed that UV line widths increased with height beyond $2 \times 10^5 K$. More elaborate study was made by Mariska, Feldman, & Doschek(1979) by examining optically thin EUV lines emitted in quiet-Sun regions above the white light limb. Their data were obtained from the NRL slit spectrograph(SO82-B) on board Skylab with $2'' \times 60''$ spatial resolution. They found that regardless of line formation temperature, nonthermal velocity increased with height from 4×10^4K to 2×10^5 K. Their typical velocity was found to be about 33km/s at $12''$ above the limb. Doschek, Feldman, & Cohen (1977), on the other hand, inferred nonthermal velocity ranging from 17 to 25km/s at the altitude of 10-20 arcsec above the coronal hole and quiet

regions. Hassler et al. (1990) analyzed MgX 609/624 coronal lines visible above 140,000km from the limb to find out that nonthermal velocity increased with height up to 70,000km.

Regarding the physical nature of nonthermal velocity, several suggestions have been made. Among them are acoustic waves(*e.g.*, Boland et al. , 1975; Mariska, Feldman, & Doschek, 1978; Cheng, Doschek, & Feldman, 1979), Alfvén waves(*e.g.*, Hassler et al. , 1990; McClements, Harrison, & Alexander, 1991, Erdélyi et al. , 1998), MHD turbulence (*e.g.*, Chae, Schüle, & Lemaire, 1998), and magnetic reconnection(*e.g.*, Chae, Schüle, & Lemaire, 1998).

Seely et al. (1997) analyzed SUMER data and found that nonthermal velocity is approximately 22km/s at 30″ above the limb and then declines to values less than 10km/s from 109″ to 209″. They also found that ion temperature was about 2.5 times larger than ionization equilibrium temperature at 109″ and 209″ above the limb, implying that the large nonthermal broadening could be caused by the discrepancy between ion and ionization equilibrium temperatures.

Studies on electron density(*e.g.*, Doyle, Banerjee, & Perez, 1998; Banerjee et al. , 1998; Peter, 1999) and center-to-limb variations of UV line intensity (*e.g.*, Mariska, Feldman, & Doschek, 1978; Roussel-Dupre, Francis, & Billings, 1979; Peter, 1999) may yield some information on the structure of the solar transition region. An earlier study on SiIV 1393/1402 lines made by Roussel-Dupré, Francis, & Billings(1979) gave a clue that the observed large nonthermal velocity and large coronal heating can not be accounted for by acoustic waves. Banerjee et al. (1998) suggested that the corona can be heated by Alfvén waves, demostrating that the nonthermal velocity was inversely proportional to the quadratic root of electron density.

In the present work, we derive total line intensity and nonthermal velocity distributions for various UV lines formed at different temperatures, using SUMER data taken during the period of May 6, 1996 through July 28, 1996. Since the observed spectral lines are emitted from the transition region within 20 arcsec above the limb, they are broadened mostly by thermal and nonthermal components.

In Section II, we describe SUMER instrument and observation. In Section III, we present data calibration procedures which include basic processes to minimize random noise, correct detector defects and convert them into physical units. In Section IV, the intensity and nonthermal velocity distributions above the limb are estimated and dependence of nonthermal broadening on height(temperature) is investigated. Emission lines obtained in quiet regions are also examined to investigate the dependence of nonthermal broadening with height. In Section V, center-to-limb variations of nonthermal velocity including the limb are carefully examined to understand their physical nature.

II. OBSERVATION AND DATA REDUCTION

(a) Instrument:SUMER

Since UV & EUV spectra can not be obtained from ground-based observatories, spectrometers were flown above the earth atmosphere. Prior to SUMER observations, the solar transition region was observed by balloons, rockets, and satellites, like NRL S082B(slit spectrograph) on SkyLab, UVSP(UV spectrometer and polarimeter) on board SMM, and HRTS(High Resolution telescope and spectrograph) on board Spacelab2. However, they do not accomodate spatial and spectral resolutions good enough and wavelength range sufficient enough to examine detailed structures of the solar transition region in contrast to the SUMER. Here important instrumental characteristics are briefly introduced. The characteristics and performance by the SUMER instrument are well described in Wilhelm et al. (1995, 1997a) and Lemaire et al. (1997) and detectors in Hollandt et al. (1996) and Wilhelm et al. (1997b).

The SUMER is a spectrometer with high spatial and spectral resolutions on board SOHO for UV & EUV spectral range. It started operating on January 1996, which is the year of solar activity minimum. It was designed to probe detail structures of the solar transition region. The SUMER covers wavelengths ranging from 400Å to 1610Å and temperatures from 10^4K to 10^6K. Four spectrometer slits are available with angular dimension of 4″ × 300″(slit 1), 1″ × 300″(slit 2), 1″ × 120″(slit 4), and 0.3″ × 120″(slit 7), respectively. They are oriented in the north-south direction. Both first and second orders of spectra are superimposed on the detector. The dispersion of emission lines depend on wavelength, varying from 45mÅ/pixel(1st order) and 22.5mÅ/pixel(2nd order) at 800Å to 41.8mÅ/pixel(1st order) and 20.9mÅ/pixel(2nd order) at 1600Å. The SUMER contains 2 detectors, A and B, only one of which is on operation at a time. Each detector contains 1024 × 360 pixels with pixel size of about $26.5\mu m \times 26.5\mu m$. The center of SUMER detector's micro channel plate is coated with KBr which raises photon detecting sensitivity by a factor of 10.

(b) Observations

To sudy the solar limb, quiet Sun spectra near north and south polar regions were taken. Some of observed spectra cover from the disk center through off the solar limb. Our SUMER data were obtained for 5 days during the period of May 6 to July 28 in 1996 with relatively long exposure time. The observation dates, related observing settings, and parameters are listed in Table 1. These data contain lines from He I, C II, C IV, N IV, N V, O IV, O V, O VI, Mg X, Si II, Si IV, S I, NeV III ions or atoms. All observed lines cover the entire temperature range of the solar transition region. Quiet regions were chosen to investigate physical characteristics of the quiet Sun limb.

Table 1. Description of data sets

Filename[a]	Lines	Det/Slit[b]	FOV(px)[c]	Exp(s)[d]
sum_960506_160924.fts	OVI 1031/1037	A/2	102 × 75	30s
sum_960506_161757.fts				
sum_960506_162630.fts				
sum_960506_163502.fts				
sum_960506_164334.fts				
sum_960506_165207.fts				
sum_960607_223404.fts	MgX 609	A/4	120 × 75	32s
sum_960707_144335.fits	NIV 765	A/2	99 × 68	60s
sum_960707_150838.fits	OV 760		99 × 68	
sum_960707_153342.fits	NeVIII 770		99 × 92	
sum_960707_155845.fits				
sum_960707_162626.fits	CII 1036/1037	A/7	71 × 32	20s
sum_960712_114143.fits	CIV 1548/1550	A/2	20 × 39	350s
sum_960707_170052.fits	HeI 584	A/7	100 × 40	60s
sum_960712_121644.fits	SiII 1533	A/2	20 × 25	
sum_960712_125144.fits	NeVIII 770		20 × 104	
sum_960712_132645.fits				
sum_960713_111135.fits	OIV 1399/1401	A/2	30 × 41	500s
	SiIV 1393/1402		30 × 37	
	SI 1401		30 × 34	
sum_960728_072012.fits	NV 1238/1242	A/2	59 × 55	60s
sum_960728_075016.fits	OV 629		59 × 55	

[a]file names indicate the time of observation, for example, sum_960506_160924.fts is observed at 16:09:24 U.T. on May 6th, 1996
[b]numbers indicate different slits. The size of each slit is 1″ × 300″(slit 2), 1″ × 120″(slit 4), and 0.3″ × 120″(slit 7). See Wilhelm et al. (1995)
[c]Full of View in pixel size
[d]Exposure time in second

(c) Data Reduction

The detector's non-uniformity yields additional uncertainty for data calibration(Wilhelm et al. , 1997b). Dark counts and scattered light also contribute undertainty. However, in the present study we avoided these problems by selecting the data points having high photon counts comparable to those of the disk center.

All the observed spectra were taken by slit 2(1″ × 300″), slit 4(1″ × 120″), and slit 7(0.3″ × 120″) so that the spatial resolution along the raster direction is less than 1 arcsec. We binned our data by 2 to 4 spatial pixels in x-direction to acquire about 3 arcsec x-directional resolution. No binning has been done toward y-direction. In the case of calibrations, however, the binning has been done to raise S/N ratio.

Here we describe data processing procedures. All the tools used for data reduction are obtained from the SUMER software tree.

i) Flattening

Due to non-uniformity of detector A, flat fielding is needed prior to analysis. In the present study we have done the flat fielding with the use of the flat field frames taken on May 15 and July 25, since most of our data were obtained in May and July.

ii) Distortion correction

The image deformation by slit slightly depends on the wavelength. The image of the slit on the detector appears shorter at the center than at edges of the detector. To correct for this geometric distortion, a distortion correcting software written by Moran(1998) has been used. The software maps the data to a rectangular grid, which have been derived from systematic observations of chromospheric lines and continua. This process corrects the distortion in the spatial direction, but it does not correct for any nonlinearity in the dispersion(Warren et al. , 1997).

iii) Gaussian fitting

Most of UV lines from the transition region are optically thin so that the Gaussian fitting method is quite efficient. The Gaussian fitting yields parameters such as total(integrated) line intensity, continuum intensity, and line width. In the present study, we have used a Gaussian fitting technique developed by Chae, Yun, & Poland(1998). The nonthermal broadening component is obtained by substracting intrinsic instrumental and thermal broadenings from observed line width. Thermal broadening components of various UV lines have been computed by using the CHIANTI database(Dere,

Table 2. Basic parameters of observed lines

line	λ^a	T(K)^b	Mass^c	Transition
C II	1036.3367	1.995e4	12.0111	$2s^2 2p\ ^2P_{\frac{1}{2}} - 2s2p^2\ ^2S_{\frac{1}{2}}$
C II	1037.0182	1.995e4	12.0111	$2s^2 2p\ ^2P_{\frac{3}{2}} - 2s2p^2\ ^2S_{\frac{1}{2}}$
C IV	1548.202	1.000e5	12.0111	$2s\ ^2S_{\frac{1}{2}} - 2p\ ^2P_{\frac{3}{2}}$
C IV	1550.774	1.000e5	12.0111	$2s\ ^2S_{\frac{1}{2}} - 2p\ ^2P_{\frac{1}{2}}$
He I	584.334	1.000e4	4.0026	$1s^2\ ^1S_0 - 1s2p\ ^1P_1$
Mg X	609.793	1.259e6	24.305	$2s\ ^2S_{\frac{1}{2}} - 2p\ ^2P_{\frac{3}{2}}$
N IV	765.147	1.585e5	14.0067	$2s^2\ ^1S_0 - 2s2p\ ^1P_1$
N V	1238.821	1.995e5	14.0067	$1s^2 2s\ ^2S_{\frac{1}{2}} - 1s^2 2p\ ^2P_{\frac{3}{2}}$
N V	1242.804	1.995e5	14.0067	$1s^2 2s\ ^2S_{\frac{1}{2}} - 1s^2 2p\ ^2P_{\frac{1}{2}}$
Ne VIII	770.409	6.310e5	20.1790	$2s\ ^2S_{\frac{1}{2}} - 2p\ ^2P_{\frac{3}{2}}$
O IV	1399.774	1.585e5	15.9994	$2s^2 2p\ ^2P_{\frac{1}{2}} - 2s2p^2\ ^4P_{\frac{1}{2}}$
O IV	1401.156	1.585e5	15.9994	$2s^2 2p\ ^2P_{\frac{3}{2}} - 2s2p^2\ ^4P_{\frac{5}{2}}$
O IV	1404.812	1.585e5	15.9994	$2s^2 2p\ ^2P_{\frac{3}{2}} - 2s2p^2\ ^4P_{\frac{3}{2}}$
O IV	1407.386	1.585e5	15.9994	$2s^2 2p\ ^2P_{\frac{3}{2}} - 2s2p^2\ ^4P_{\frac{1}{2}}$
O V	629.730	2.512e5	15.9994	$2s^2\ ^1S_0 - 2s2p\ ^1P_1$
O V	760.445	2.512e5	15.9994	$2s2p\ ^3P_2 - 2p^2\ ^3P_2$
O VI	1031.924	3.162e5	15.9994	$2s\ ^2S_{\frac{1}{2}} - 2p\ ^2P_{\frac{3}{2}}$
O VI	1037.614	3.162e5	15.994	$2s\ ^2S_{\frac{1}{2}} - 2p\ ^2P_{\frac{1}{2}}$
S I	1401.5138	1.000e4	32.06	
Si II	1533.431	1.259e4	28.0860	$3s^2 3p\ ^2P - 3s^2 4s\ ^2S$
Si IV	1393.755	6.310e4	28.0860	$3s\ ^2S_{\frac{1}{2}} - 3p\ ^2P_{\frac{3}{2}}$
Si IV	1402.770	6.310e4	28.0860	$3s\ ^2S_{\frac{1}{2}} - 3p\ ^2P_{\frac{1}{2}}$

[a]from CHIANTI Database
[b]from CHIANTI Database
[c]atomic weight from Allen(1973)

et al. , 1997), which are listed in Table 2.

The Gaussian fitting function is described as

$$I_{fit}(\lambda) = a_o + a_1\lambda + a_2\lambda^2 + \sum_i I_p^i exp\left[-\frac{1}{2}\left(\frac{\lambda-\lambda_c^i}{\Delta\lambda_D^i}\right)^2\right] \quad (1)$$

where $\Delta\lambda_D^2$ is given by

$$\Delta\lambda_D^2 = \frac{\lambda^2}{c^2}\left(\frac{2kT_i}{M_i} + \xi^2\right) + \Delta\lambda_I^2. \quad (2)$$

with nonthermal velocity ξ and instrumental broadening $\Delta\lambda_I$.

Here we assume that T_i is equal to electron temperature T_e. The ionization equilibrium temperature for each ions have been taken from CHIANTI database, which is based on Arnaud & Rothenflug(1985). The intrinsic instrumental width has been taken as 2.3 pixels, following Wilhelm et al. (1997a) and Chae, Schühle, & Lemaire(1998).

iv) Radiometry

To convert photon counts to physical units, radiometering process is required. Radiometrical calibration has been done by Hollandt et al. (1996) before loading SUMER on board SOHO in the laboratory. According to Wilhelm et al. (1997a), in-flight calibration indicates that the radiometric calibration is still valid within $\pm 15\%(1\sigma)$ at short wavelength and $\pm 30\%$ at larger wavelength(see Wilhelm et al. , 1997b and Hollandt et al. , 1996 for further details). In the present work the radiometric calibration has been processed with the use of RADIOMETRY.PRO of the SUMER software package, where we have used 15% as uncertainty in the intensity calibration.

(d) Data Selection and Distribution Plot

For flat field correction, distortion correction, and radiometry calibration, the photon counts of each pixel were carefully examined, and regions of high photon counts were carefully selected apropos to the counts of disk center. High photon counts permit us to exclude problems such as scattered light. To select physically meaningful data points, the following criteria have been

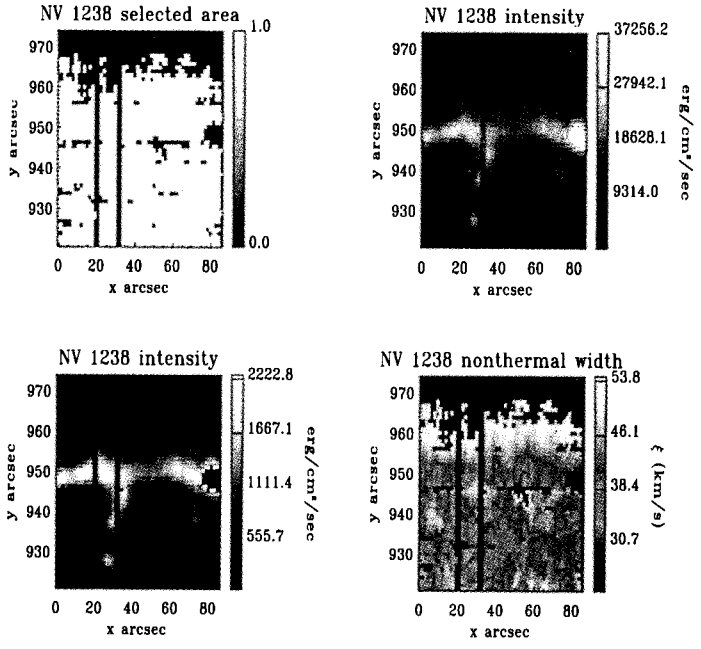

Fig. 1.— Example of data selection for NV 1238. Selected pixels correspond to white area in the left top image. The right top is intensity image for all data and the bottom images show intensity and nonthermal velocity maps represented by selected pixels.

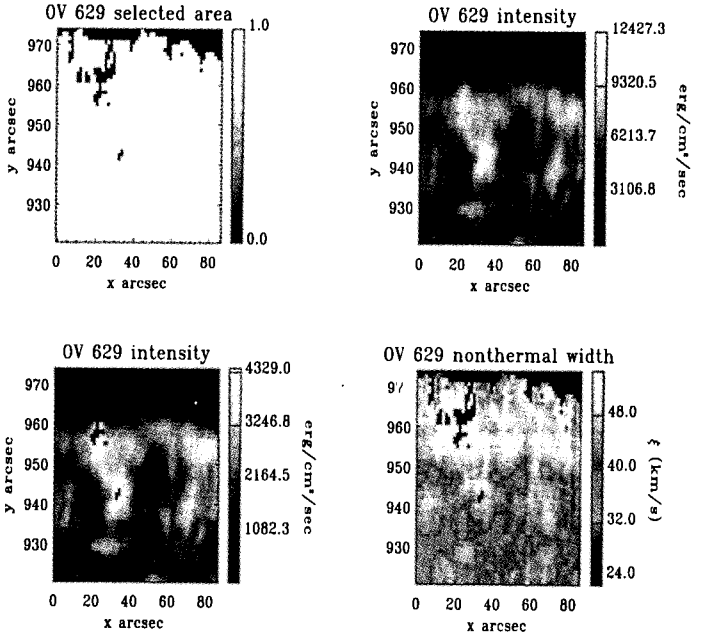

Fig. 2.— Example of data selection for OV 629. White area in the left top image refers to selected pixels. The rest is the same as in Fig. 1.

set up for the present work.

1. Spectral lines with too low peak intensity are omitted: we select data points with Gaussian profile having line peak intensity commensurate to that of disk center.
2. Spectral lines with extremely large nonthermal velocity are omitted: nonthermal velocities larger than 2σ are dismissed to get rid of lines associated with multiple flows or jets.
3. Spectral lines with extremely high value of total intensities are omitted: total intensities larger than 3σ are dismissed to get rid of improperly overestimated lines in active regions.
4. Only optically thin doublet line pairs are selected by requiring that intensity line ratio of doublets should be larger than 85% of theoretically predicted value to secure optically thinness.
5. Only strips in which the number of qualified data points(which pass the first 4 criteria) exceed 70% of the total, are selected for analysis.
6. Only quiet Sun regions are considered by taking observed total line intensities which do not exceed 50% of the spatially averaged intensity over the region under consideration.

Every pixel was processed by the above criteria. Fig. 1 and Fig. 2 show samples for a doublet N V 1238 line and for a non doublet O V 629 line respectively, where the dark pixels refer to data points which fail to pass the criteria. White area in the figures on the upper left corner of Fig. 1 and Fig. 2 represent the pixel points which satisfy the first 4 criteria listed above. Most of dark pixels are located off the limb, where the intensity is too low and/or optical depth is too large. We also made image maps of total intensity and nonthermal velocity from all emission lines selected for the present analysis.

After composing image maps, total line intensity and nonthermal velocity evaluated at individual data points of each UV lines have been averaged horizontally at each height to derive vertical distribution above the limb. They are presented in Fig. 3, where the figures on the left column refer to total line intensity variation of observed UV lines and on the right, to nonthermal velocity variation with height. In the figures dotted vertical lines refer to a location where the limb brightening of each UV lines maximizes and dashed vertical lines, to a location at which continuum nearby each UV lines maximizes. The dash-dotted vertical lines refer to a location where the total line intensity is cut down by $1/e$.

As can be seen from Fig. 3, a majority of the observed lines reveals considerable limb brightening, and their total line intensity distributions are well represented by exponential fuction. It is interesting to note that UV lines which do not show large limb brightening are found to be optically thick, as evidenced from He I,

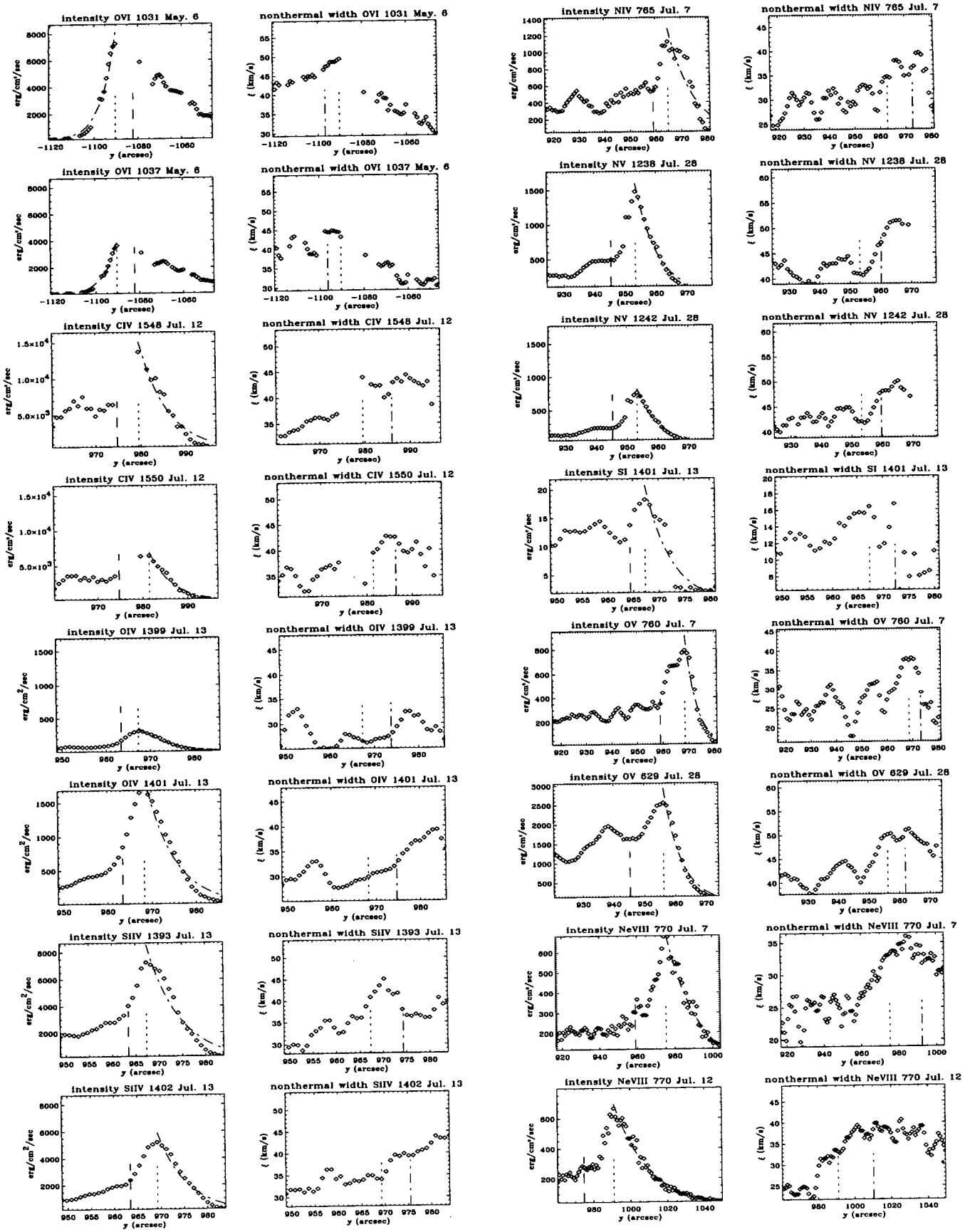

Fig. 3.— Intensity(left) and nonthermal velocity (right) as a function of height. Dashed lines refer to a location at which continuum near individual UV lines maximizes,dotted lines to a location at which limb brightening of lines maximizes, total line intensity distribution is cut down by 1/e.

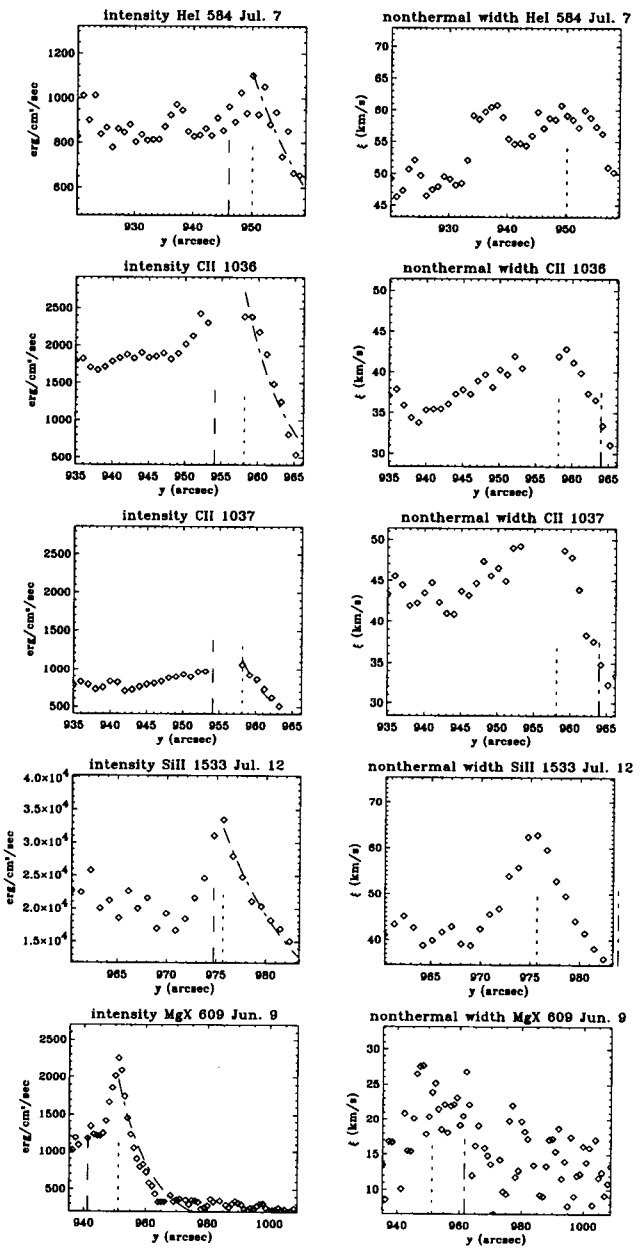

Fig. 3.— *Continued*

C II, and Si II lines. This is consistent with characteristics of optically thick lines, in the sence that optically thick line has a shorter path length, which leads to weak limb brightening. Accordingly, in the present study we excluded optically thick He I, C II, Si II lines for analysis.

III. THE STRUCTURE OF THE QUIET LIMB

(a) Limb Brightening

Even though the FITS header of each datum contains instrumental pointing coordinate in arcsec, it does not seem to represent the true solar limb. Wilhelm et al. (1998) indicated that the solar radius, $R_\odot$, in angular dimension has been varied from 954″ to 986″ during several months of observations. Tu et al. (1998) mentioned that SUMER cannot determine the photospheric limb. No limb position can be inferred from each datum header. In the present work we defined the "line limb" as a position at which total line intensity of each individual observed UV lines maximizes. To measure the height of the line limb, a reference height has to be defined as a zero point. In the present work we defined the reference height as a position at which the continuum near each individual lines maximizes. The resulting line limb heights of individual lines are listed in the fifth column of Table 3, where the third and the fourth columns refer to locations of line peak and continuum intensity peak, respectively. As seen from the figure, the peak position of the total line intensity increases with temperature(height) as expected. This is in line with Mariska & Withbroe(1975), Nicolas et al. (1977), and Kjeldseth-Moe & Nicolas(1977).

(b) Line Intensity Scale Height

Total line intensity scale heights for individual observed UV lines have been estimated from the figures on the left column of Fig. 3 (or the left figure of Fig. 4.) by fitting the deduced intensity distributions to exponential function. The resulting scale heights of optically thin UV lines are listed in the third column of Table 4, which are plotted against temperature in Fig. 5. As seen from the figure, they do not vary much with height up to $2 \times 10^5 K$. Only Ne VIII line has larger scale height than others, namely about 17 arcsec above the continuum limb.

Several studies have been made to estimate intensity scale height. Nicolas et al. (1977) suggested a scale height of about 1500km, Kjeldseth-Moe & Nicolas(1977), between 1750km and 3500km comparable to H_α spicule size. Feldman, Doschek, & Patterson(1976) analyzed total line intensity distributions of various lines above the limb and found that they fall to half-maximum intensity within less than 4 arcsec outside from the limb. This means that one scale height equals to about 6″, which is quite similar to ours, as seen from Fig. 5.

The temperature-independent line intensity scale

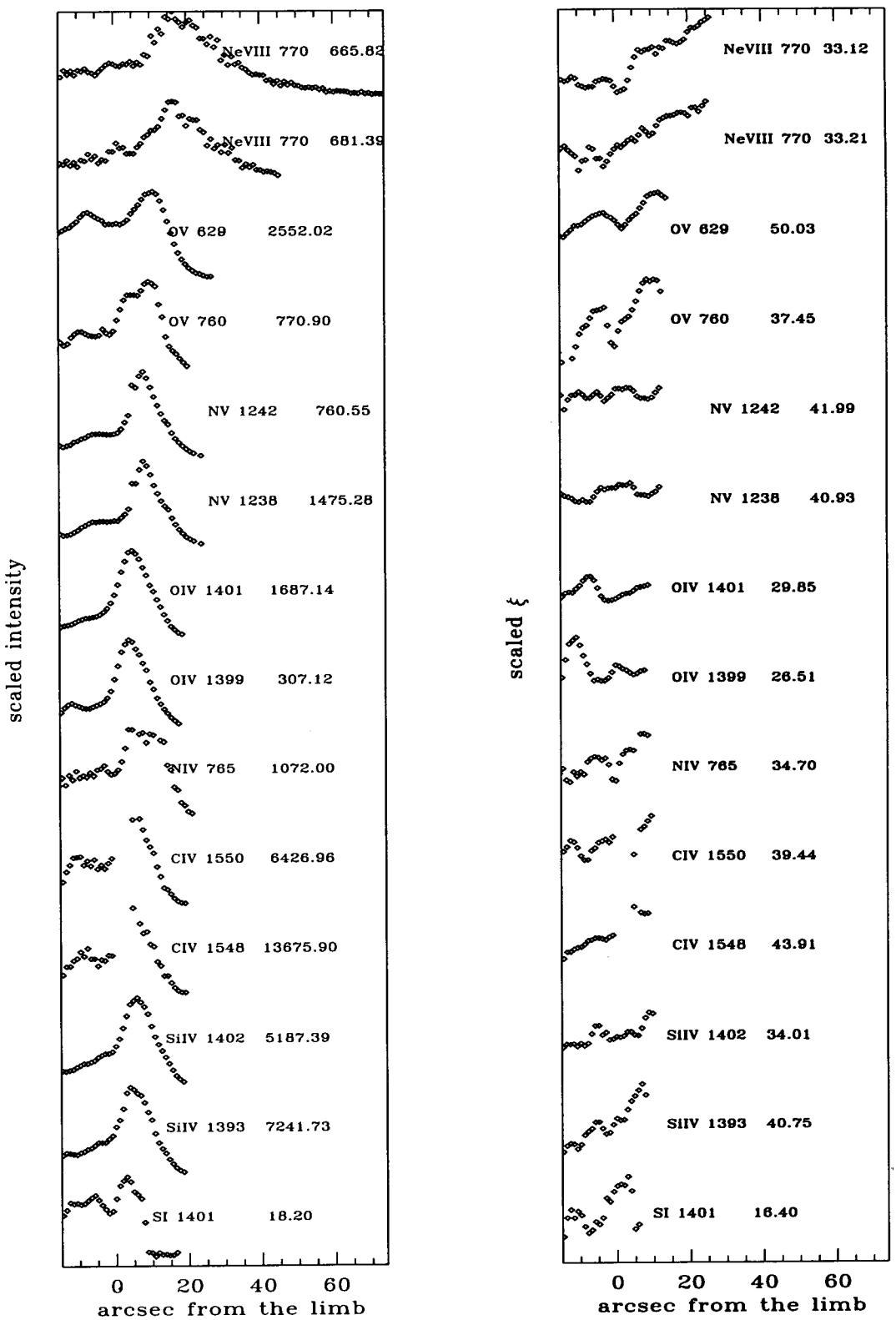

Fig. 4.— Scaled plot of intensity(left) and nonthermal velocity(right). Note that each line intensity peak increases with height.

Table 3. Locations of continuum limb($Y_{limb}{}^b$) and line limb($Y_p{}^a$)

Ion	λ	$Y_p{}^a$	$Y_{limb}{}^b$	ΔY ($Y_p{}^a - Y_{limb}{}^b$)	Date
MgX	609	951.150	941.211	9.939	Jun. 7
HeI	584	950.133	946.139	3.994	Jul. 7
OV	760.4	968.587	958.971	9.616	Jul. 7
NIV	765	964.741	958.971	5.770	
NeVIII	770	975.318	958.971	16.347	
CII	1036	958.154	954.115	4.039	Jul. 7
CII	1037	958.154	954.115	4.039	
CIV	1548	979.529	974.738	4.791	Jul. 12
CIV	1500	981.445	974.738	6.708	
SiII	1533	975.696	974.738	0.958	
NeVIII	770	992.027	974.738	16.289	
SiIV	1393	967.313	963.411	3.902	Jul. 13
SiIV	1402	969.264	963.411	5.853	
SI	1401	966.336	963.411	2.927	
OIV	1393	967.313	963.411	3.902	
OIV	1401	968.288	963.411	4.877	
OV	629	956.203	945.290	10.913	Jul. 28
NV	1238	953.226	945.290	7.936	
NV	1242	953.226	945.290	7.936	
OVI[¶]	1031	-1090.38	-1082.31	8.072	May. 6
OVI	1037	-1090.38	-1082.31	8.072	

[a]y-coordinate of line intensity peak(line limb)
[b]coordinates of each line's continuum peak(continuum limb)
[c]south limb observation

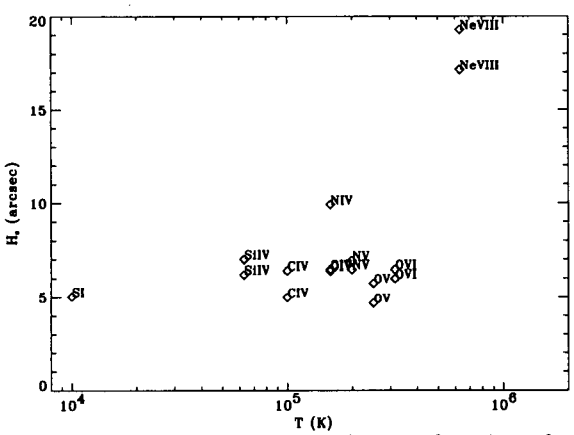

Fig. 5.— Line intensity scale height as a function of temperature

height can be understood in terms of 1) a steep temperature gradient of the solar transition region and 2) possible unseen features whose size is less than one intensity scale height. As is well known, the transition region has very steep temperature gradient, where the temperature varies from 10^4K to 10^6K within one thousand kilometer. The near constant temperature gradient could result in temperature-independent intensity scale height. Regarding the latter possibility, some conjectures can be suggested. Spicules or similar sized loop structures are not resolved spectroscophically. Then, the unresolved structures are likely to contribute coronal heating below the region of 2×10^5K, which results in temperature-independent intensity scale height.

The intensity scale height estimated from Ne VIII lines is quite different from others, which could be due to the lower and upper transition regions being quite different from each other as suggested by Mariska & Withbroe(1975), Withbroe & Mariska(1976), Nicolas et al. (1977), and Mariska, Feldman, & Doschek(1978). According to Chae, Yun, & Poland(1998) magnetic flux tubes expand rapidly upward, starting from 2×10^5K, which differentiate physical conditions between the lower and upper transition regions.

(c) Nonthermal Velocity above the Limb

Nonthermal velocity distributions for each observed lines have been deduced, which are plotted as a function of limb positions in the right side of Fig. 3 and Fig. 4. As can be seen from the figures, no nonthermal velocity distribution decrease above the continuum limb up at least to one intensity scale height. Beyond the line limb, little correlation is found between intensity and nonthermal velocity.

One of the early limb profile observations performed by Shine et al. (1976) showed that the Gaussian width of observed UV lines increased up to about 5 arcsec beyond their respective line limb even though their line

Table 4. Estimated total line intensity scale height and nonthermal velocity

Ion	λ	$H_o(arcsec)$	$\xi \pm \sigma_\xi$	Date
MgX	609	10.447	21.608±1.021	Jul. 7
OV	760.4	4.594	37.076±2.721	Jul. 7
NIV	765	9.911	30.477±1.354	
NeVIII	770	17.134	34.154±0.389	
CIV	1548	6.415	34.179±0.552	Jul. 12
CIV	1500	4.983	40.931±0.604	
SiII	1533	8.187	26.566±1.257	
NeVIII	770	19.281	35.746±0.345	
SiIV	1393	7.010	42.719±1.352	Jul. 13
SiIV	1402	6.204	37.352±0.488	
SI	1401	5.031	13.714±2.199	
OIV	1393	6.479	26.566±1.257	
OIV	1401	6.405	30.576±0.448	
OV	629	5.736	49.606±1.537	Jul. 28
NV	1238	6.938	41.605±0.986	
NV	1242	6.479	42.806±0.883	
OVI	1031	6.479	48.835±0.833	May. 5
OVI	1037	5.984	44.224±0.651	

intensities decreased. C IV 1548/1550 observations showed that nonthermal velocity varies from 28km/s on the disk center to 35km/s off the limb, which was also found by the NRL slit spectrograph(S082-B) on board Skylab by Mariska, Feldman, & Doschek(1979). Even at low resolution, all nonthermal line broadenings obtained by S082-B showed systematical increase with height, common to different UV lines, like O V lines(Vial et al. , 1980) and Mg X 609/625 lines(Hassler et al. , 1990). These are also in line with our results.

(d) Relation between Physical Parameters of the Limb

i) T - ξ and ΔY - ξ

The relation between temperature and nonthermal velocity has been analyzed. Fig. 6 shows nonthermal velocities estimated from the UV lines observed off the limb, where they are compared with those on the disk center measured by Chae, Schühle, & Lemaire(1998). As seen frome the figure, the nonthermal velocity above the limb is systematically larger than that of the disk center except for coronal lines. However, their pattern is very similar to each other in that their peak is located around $2 \times 10^5 K$.

We may note that our result is quite similar to that of Kjeldseth-Moe & Nicolas(1977), except for O IV where the nonthermal velocity is about 10km/s, much smaller than that of other lines formed in similar temperature. However, Kjeldseth-Moe & Nicolas(1977) also obtained nearly identical nonthermal velocity as ours. Doyle et al. (1997) claims that intersystem line(spin change), like O IV($1.6 \times 10^5 K$) yields nonthermal velocity somewhat lower(*e.g.*, 10-12km/s).

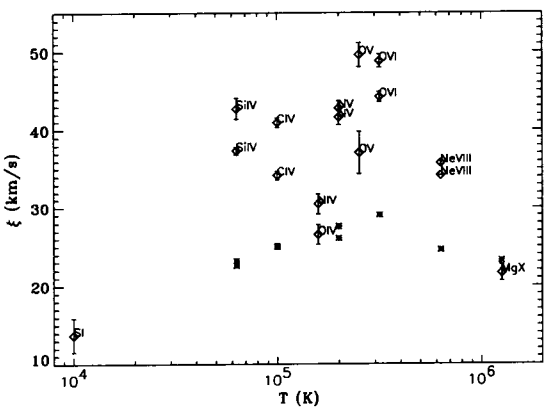

Fig. 6.— ξ estimated at the line limb is plotted against temperature of line formation. In the figure * refers to ξ of the disk obtained by Chae, Schühle, & Lemaire(1998).

In addition we plotted measured nonthermal velocities from various UV lines against ΔY in Fig. 7, where ΔY refers to the distance between line limb and continuum limb of each observed lines.

ii) ΔY - T

With the use of Fig. 6 and Fig. 7, Y versus T plot is obtained, which is shown in Fig. 8. Since the value of Y is not so exact that the definitive power relation between height and temperature cannot be determined. However, a rough relation between ξ and ΔY is useful for modelling higher solar atmospheres. It should be noted that most solar model atmospheres end at the

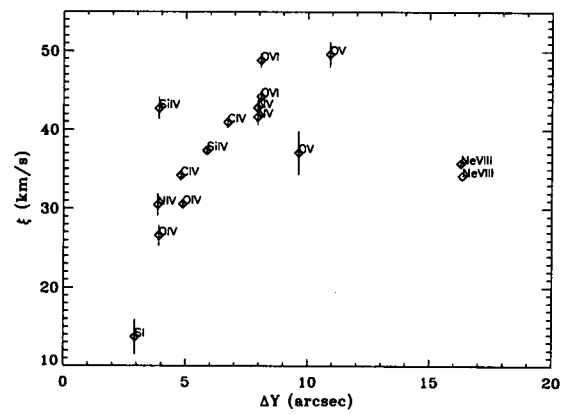

Fig. 7.— ξ estimated at the line limb is plotted as a function of ΔY, where ΔY is the distance between continuum and line limbs.

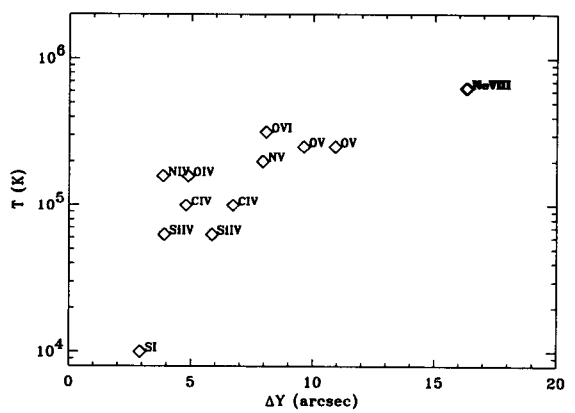

Fig. 8.— T vs. ΔY for various UV lines. ΔY refers to height of line limb which is measured from continuum limb. T refers to ionization temperature.

upper chromosphere(*e.g.*, Vernazza, Avrett, & Loeser, 1981).

iii) $\Delta\xi$ between disk and limb

Fig. 9 shows how the nonthermal velocity off the limb differs from that of the solar disk center. Our result is quite different from that of Erdélyi et al. (1998), in the sense that their $\Delta\xi$ are randomly distributed so that no correlation is found between temperature and $\Delta\xi$. As can be seen from Fig. 9, however, our $\Delta\xi$ distribution is peaked in the middle of the transition region, as nonthermal velocity distribution of the disk center is(see Fig. 6).

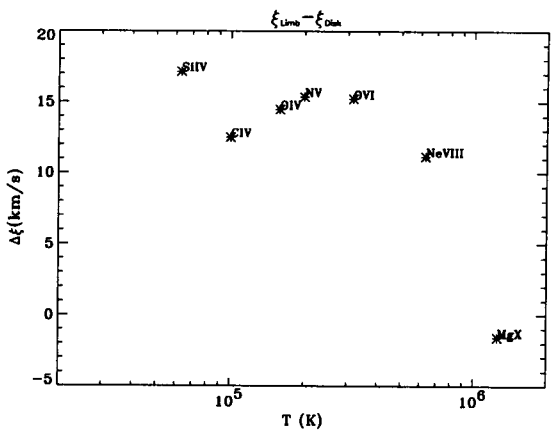

Fig. 9.— $\Delta\xi$ vs. T for various UV lines. $\Delta\xi$ is the difference in nonthermal velocity measured at line limb and disk center. Here the value of ξ at the disk(*) is adopted from Dere & Mason(1993) for O IV line data and Chae, Schühle, & Lemaire(1998) for other lines.

(e) Electron Density and Alfvén Wave above the Solar Limb

i) Electron density measurement

The oxygen lines, O IV 1399/1401 (*e.g.*, Dwivedi, 1994) and O V 760/629 (Wilhelm et al. , 1995) can be applied for density diagnostics. Since O IV 1399 is very weak and is located at the edge of detector where distortion is most serious, hence O IV 1399/1401 line pair is not a good candidate for electron density diagnostics. Thus, we have used O V 760/629 lines for density diagnostics for the quiet solar limb even though these line pairs are observed on different days.

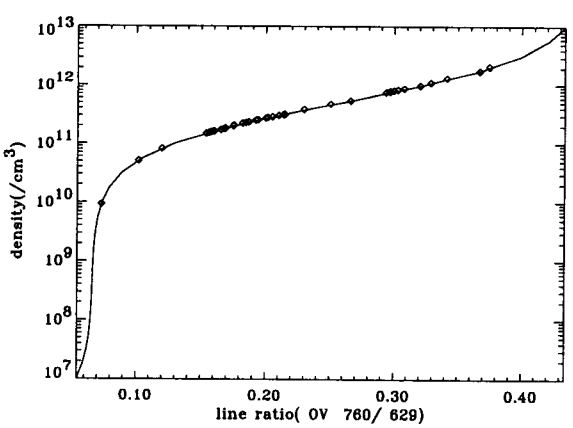

Fig. 10.— Line ratio vs. electron density. The solid line represents the computed result from CHIANTI database and rhombi, observed points.

Line ratio is related to electron level population. Electron level population is ruled by plasma electron density. This allows to calculate electron density from

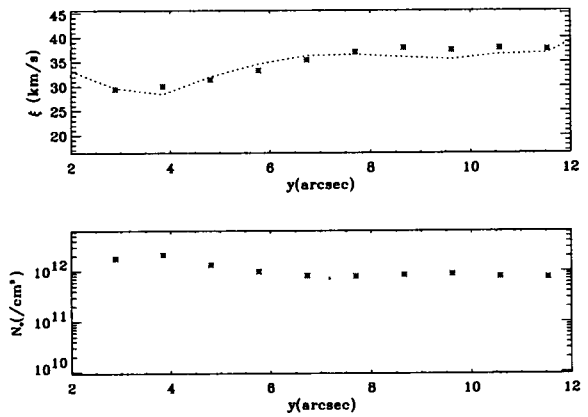

Fig. 11.— Nonthermal velocity and electron density estimated in the neighborhood of O V 760 line limb. The dotted line refers to a theoretically predicted functional form given by Eq.4

line ratio(see Dwivedi,1994). With the aid of CHIANTI software written by Dere et al. (1997) and Landi et al. (1999), the relation between the line intensity ratio of O V 760/629 and electron density has been obtained, which is shown in Fig. 10. The electron density estimated from the figure ranges from $1 \times 10^{10} cm^{-3}$ to $2 \times 10^{12} cm^{-3}$. We also plot ξ against height, Y in Fig. 11, where the zero point of Y has been set to the continuum limb of OV 760. As seen from Fig. 11, the density at 2 arcsec below at the line limb is found to be $2 \times 10^{12} cm^{-3}$, but it decreases to $5 \times 10^{11} cm^{-3}$ at one scale height above the line limb. Finally, it is noted that our estimates are comparable to those of Kjeldseth-Moe & Nicolas(1977) who obtained $N_e \simeq 10^{11} cm^{-3}$ at $5 \times 10^4 K$ from Si III line near 1300Å.

ii) Alfvén wave

With the use of Fig. 11 we have deduced a relation between nonthermal velocity and electron density, which are shown in Fig. 12. The derived nonthermal velocity is found to be approximately proportional to an inverse of quadratic root of electron density; $\xi \sim {N_e}^{-0.256}$. This is very interesting because it supports a notion that nonthermal velocity is originated from Alfvén waves passing through medium, as can be seen from the following theoretical consideration.

Suppose that nonthermal energy flux density comes from waves propagating through the solar atmosphere. Then, the flux can be expressed as $F = n_e m_p < V_h^2 > v$. If the nonthermal energy flux primarily comes from Alfvén waves, then the flux is given by

$$F = \sqrt{\frac{\rho}{4\pi}} < \delta v^2 > B \qquad (3)$$

(Doyle et al. , 1997), where ρ is the plasma mass density(related to N_e as $\rho = m_P N_e$, where m_P is proton

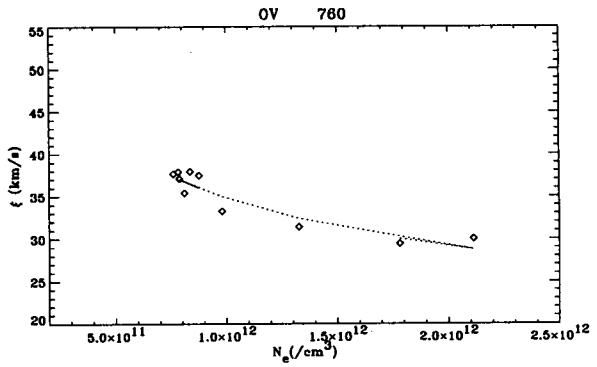

Fig. 12.— Electron number density vs. nonthermal velocity at the line limb of O V 760. The dotted line is represented by $\xi \propto \rho^{-0.256}$.

mass) and $< \delta v^2 >$ is the mean square velocity obtained from observation. $< \delta v^2 >$ is equal to $2 < V_h^2 >$, when random polarization is assumed. B is the magnetic field strength, and v_A is equal to $B/\sqrt{4\pi\rho}$. Since F is constant with height, $< \delta v^2 >^{1/2}$ can be rewritten as

$$< \delta v^2 >^{\frac{1}{2}} \propto \rho^{-\frac{1}{4}}. \qquad (4)$$

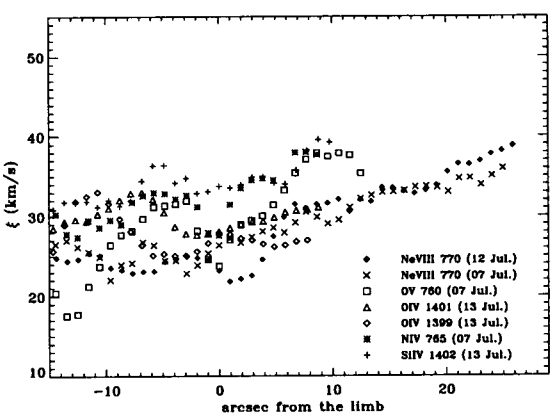

Fig. 13.— Nonthermal velocity variation with height for intersystem and forbidden UV lines. Their nonthermal velocities are found to be less than 35km/s.

Finally, we have tested whether or not nonthermal velocity varies with height above the limb. For this purpose we plotted ξ at the line limb against line formation height, which is measured from the continuum limb of each individual UV lines. They are shown in Fig. 13 and Fig. 14. Here we grouped them into two, one of which comprises UV lines whose ξ yields less than 35km/s at their line limb(Fig. 13) and the other of which comprises UV lines whose ξ is larger than 35km/s(Fig. 14). It is interesting to note that the first group belongs to forbidden and intersystem lines and the second group, to resonance lines. At present

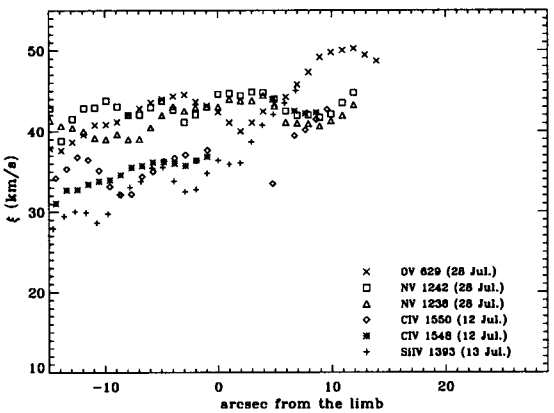

Fig. 14.— Nonthermal velocity variation with height for resonance UV lines, such as N V, C IV, Si IV. Their nonthermal velocities at the line limb are found to be greater than 35km/s.

we are not sure why ξ estimated from intersystem and forbidden UV lines is systematically much lower than resonance UV lines.

Table 6. Radial and tangential components of the nonthermal velocity

Ion	$V_r \pm \sigma_{V_r}$	$V_t \pm \sigma_{V_t}$
S I 1401	5.933 ± 0.053	7.250 ± 0.095
Si II 1533	18.735 ± 0.043	24.597 ± 0.077
Si IV 1393	21.759 ± 0.049	26.739 ± 0.102
Si IV 1402	23.832 ± 0.032	28.512 ± 0.068
C IV 1548	25.030 ± 0.048	30.515 ± 0.084
C IV 1550	26.824 ± 0.032	31.759 ± 0.057
O IV 1399	22.259 ± 0.044	27.657 ± 0.080
Ne VIII 770	24.856 ± 0.043	28.977 ± 0.080

IV. CENTER-TO-LIMB VARIATIONS

(a) Center-to-Limb Variation of Total Line Intensity

We analysized ceneter-to-limb variations of total line intensity and nonthermal velocity of various UV lines to understand the transition region structure. The observed data are summerized in Table 5, where instrumental setup, observing dates, exposures are described. To analyze center-to-limb variation, optical depth problem has to be resolved prior to analysis. Upon selecting optically thin data points, we have computed total line intensity at each selected data points. Optically thin data points are obtained by employing data selection criteria(see Section 3.2). Spatial averaging has been made over about 30 arcsec in x-direction for each line. The deduced center-to-limb variations were

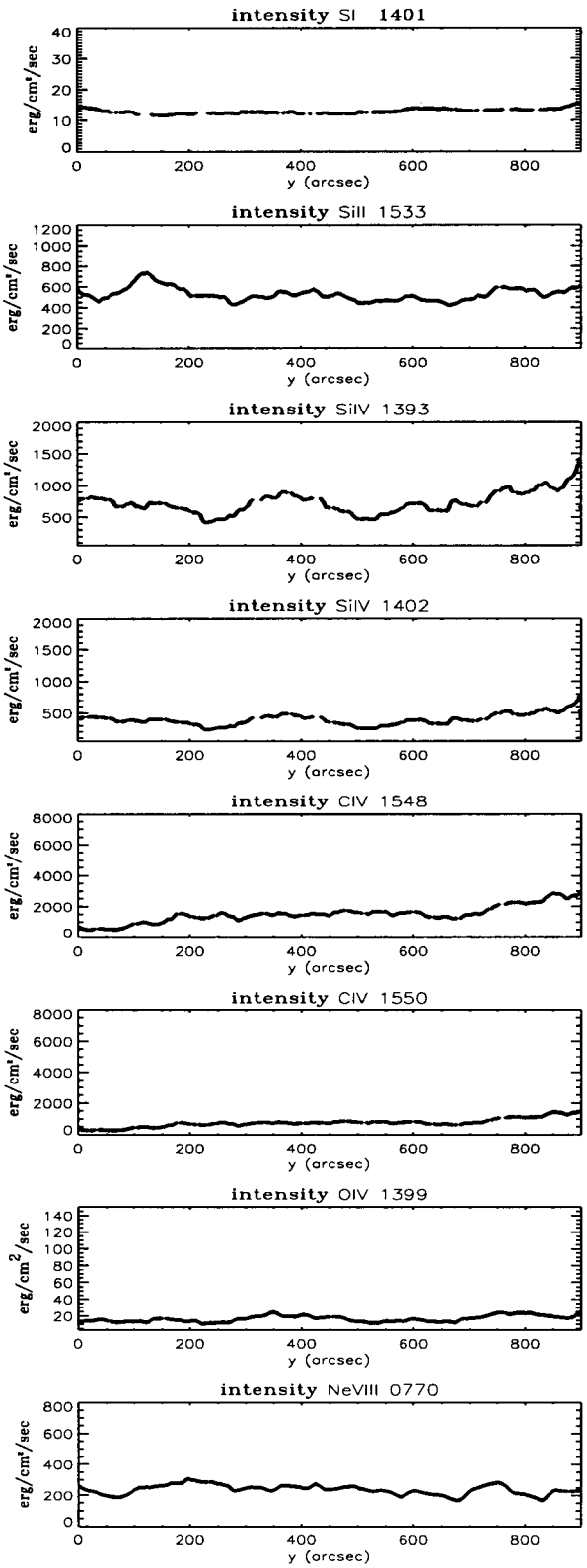

Fig. 15.— Center-to-limb intensity variation of various UV lines considered

Table 5. Descrition of data set for center-to-limb observations

Filename	Y[a]	Det/Slit[b]	Lines	FOV(px)	Exp
sum_960712_021710.fits	0.″	A/2	CIV 1548/1550	30 × 313	350s
sum_960712_025211.fits			SiII 1533		
sum_960712_032712.fits			NeVIII 770		
sum_960712_040213.fits					
sum_960712_043714.fits					
sum_960712_054842.fits	300.″	A/2	CIV 1548/1550	24 × 313	350s
sum_960712_062343.fits			SiII 1533		
sum_960712_065844.fits			NeVIII 770		
sum_960712_073345.fits					
sum_960712_092012.fits	600.″	A/2	CIV 1548/1550	21 × 313	350s
sum_960712_103014.fits			SiII 1533		
sum_960712_110514.fits			NeVIII 770		
sum_960712_114143.fits	900.″	A/2	CIV 1548/1550	21 × 243	350s
sum_960712_121644.fits			SiII 1533	21 × 227	
sum_960712_125144.fits			NeVIII 770	21 × 296	
sum_960712_132645.fits					
sum_960712_221207.fits	0.″	A/2	OIV 1399/1401	30 × 304	500s
			SI 1401		
			SiIV 1393/1402		
sum_960713_023157.fits	300.″	A/2	OIV 1399/1401	30 × 304	500s
			SI 1401		
			SiIV 1393/1402		
sum_960713_065146.fits	600.″	A/2	OIV 1399/1401	30 × 304	500s
			SI 1401		
			SiIV 1393/1402		
sum_960713_111135.fits	900.″	A/2	OIV 1399/1401	30 × 238	500s
			SI 1401	30 × 238	
			SiIV 1393/1402	30 × 239	

[a]slit center position pointing y-direction
[b]refer Table 2

smoothed by taking a running average over 80 pixels(corresponding to the twice size of super granules) to reduce fluctuations caused by solar features. The resulting center-to-limb variations are shown in Fig. 15. As seen from the figure, there are no dramatic intensity variations. Only C IV, Si IV, and O IV show a slight increase in intensity toward the limb. These ions occupy the middle transition region. Weak intensity variations toward the limb are noted in Fig. 15.

According to Peter(1999) the intensity contrast of coronal hole against the quiet Sun is found to be about 50%. Since our slit were oriented along N-S direction, our reduced center-to-limb variations could be biased by polar coronal holes, which may result in weak center-to-limb variations especially toward the limb.

(b) Center-to-Limb Variation of Nonthermal Velocity

It is more difficult to analyze center-to-limb variation of nonthermal velocity. Since opacity effect increases gradually toward the limb, it is not sure whether the center-to-limb variation is due to directional dependence of nonthermal velocity or due to broadening solely by opacity.

The center-to-limb variations of nonthermal velociy deduced from various UV lines are presented in Fig. 16. After smoothing, all the data points are well fitted with radial and tangential velocity components. The solid and dotted lines in the figures represent curves fitted to the observations by least square method with linear and trigonometric functions, respectively. The trigonometric functional fitting is introduced to examine which component of nonthermal velocity, *e.g.*, horizontal or vertical influences the center-to-limb variation more effectively. As seen from the figures and also from Table 6, the tangential flow motion is systematically more dynamical than the radial motion. For the case of C IV, however, our result is quite contradictory to Peter(1999). Peter(1999) argued that inside the limb nonthermal velocity of C IV line decreases by about 20% and increases rapidly near the limb due to opacity effect. Since all the optically thick data points have been eliminated in our analysis, our results should not be influenced by the opacity effect.

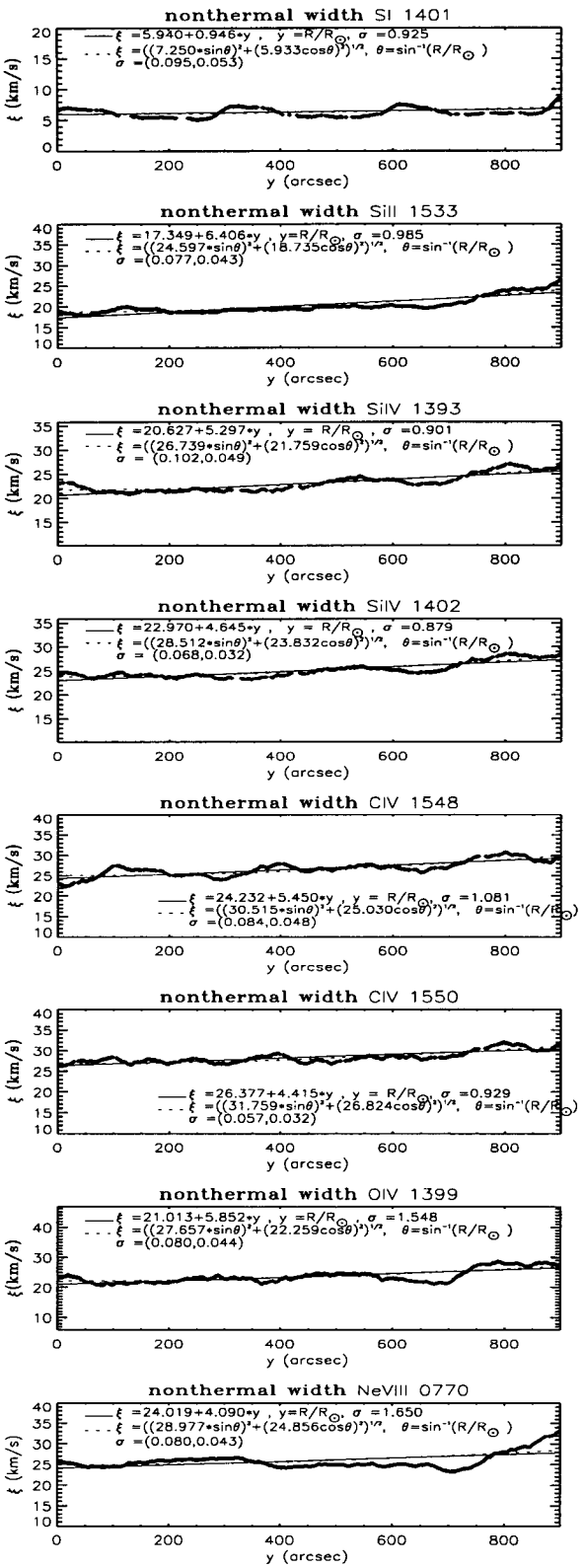

Fig. 16.— Center-to-limb nonthermal velocity variation. The solid lines refers to linear least square fitting, while dotted lines to least square fitting by trigonometric function.

The cause for center-to-limb variation of nonthermal velocity can be interpreted in two ways. One is that the center-to-limb variation comes from non-isotropic mass flows which are unresolved by observations. The other could be due to just LOS effect. The superposition of the unresolved fine structures contributes to line broadening. The former seems reasonable when the morphology of magnetic field in the transition region is considered. According to Chae, Yun, & Poland(1998) the magnetic flux tube expands upward very rapidly, starting from $2 \times 10^5 K$. We may speculate that loop structures could be easily formed and magnetic reconnection could take place more frequently due to flux tube expansion, which may cause considerable nonthermal broadening.

V. SUMMARY AND CONCLUSION

In this study we have made a spectroscopic study of the solar transition region using high resolution UV & EUV data obtained by SUMER on board SOHO. Optically thin and conspicuous emission lines observed at the solar limb are carefully selected to derive nonthermal velocity of the transition region. The data used in this work were observed for 5 days during the period of May 6 through July 28, 1996. They contain spectra covering the entire north and south polar regions to examine center-to-limb variations and to investigate physical characteristics off the limb.

To study limb structures quiet Sun spectra were taken by placing the slit in north-south direction beyond the limb. For this purpose we selected data points very carefully by avoiding spectral lines whose intensity is too low to fit to Gaussian profile and whose width are excessively large enough to include data points containing multi-flows or jets. For doublet lines we carefully selected optically thin data points by evaluating the intensity ratio prior to analysis. With the use of carefully selected data points total line intensities and nonthermal velocities have been estimated. Total line intensity distributions of all the observed UV lines have been deduced and their corresponding nonthermal velocity distribution have been computed, which are presented in Fig. 3 and Fig. 4.

To examine limb brightening distribution of total line intensity with height, a reference zero point should be defined. For this purpose we defined "line limb" and "continuum limb". The line limb is defined as a location at which the total line intensity of individual UV lines maximizes and the continuum limb, as a location at which the continuum near individual UV lines maximizes. The distance between line limb and continuum limb defines the line formation height of individual observed UV lines.

With the use of prudent information we obtained, we examined the characteristics of total intensity and nonthermal velocity distributions with height together with those of center-to-limb variation. Several important findings emerged from the present work are as fol-

lows.

First, most of UV & EUV lines are optically thin so that steep limb brightenings are detected at intensity distribution off the limb. C II, Si II, and He I, lines are found to be optically thick. However, most of the observed lines including forbidden and intersystem lines are found to be optically thin.

Second, nonthermal velocity off the limb are systemically greater than that of the disk. The discrepancy between the disk and the limb maximizes at 2×10^5K. Their variations with temperature are also similar to each other, implying that the mechanism of nonthermal line broadening does not depend on the direction but on LOS effect. Isotropic nano flare heating or turbulence heating seems to make significant contribution to nonthermal line broadening near 2×10^5K.

Third, it is found that the intensity scale heights estimated from different lines are nearly identical to each other in the lower temperature region, implying that the same heating mechanism can be applicable to the region. The deduced scale heights are found to be almost the same as that of spicules, which supports a notion that the lower transition region part contains spicule-like or small loop-like structure.

Fourth, the analysis of O V 760/629 yields density ranging from $10^{10} cm^{-3}$ to $2 \times 10^{12} cm^{-3}$. Though nonthermal velocity and electron density are deduced from different methods, excellent linearity is found between inverse quadruple root of electron density and nonthermal velocity. This means nonthermal broadening favors heating by undamped, radially propagating Alfvén waves.

Finally, our deduced center-to-limb variation of nonthermal broadening suggests that the tangential(horizontal) component of nonthermal velocity is systematically larger than that of the radial(vertical) component. This reveals that the morphology of the transition region can be raveled with nonisotropic mass flows, which is different from the results based on isotropic nano flare and magnetic turbulence heatings. Unisotropic unresolved flows also seem to be dominant near $2 \times 10^5 K$.

We woud like to thank the members of the SUMER team for technical support and T. Moran for providing the data for detector geometric distortion. This work is supported partially by Korea-U.S. Cooperative Science Program under KOSEF(995-0200-004-2) and by BSRI-98-5408.

REFERENCES

Allen, C. W. 1973, 3rd Ed., The Athlone Press. LTD

Arnaud, M., & Rothenflug, R. 1985, A&AS, 60, 425

Banerjee, D., Teriaca, L., Doyle, J. G., & Wilhelm, K. 1998, A&A, 339, 208

Boland, B. C., Dyer, E. P., Firth, J. G., Gabriel, A. H., Jones, B. B., Jordan, C., McWhirter, R. W. P., Monk, P., & Turner, R. F. 1975, MNRAS, 171, 697

Boland, B. C., Engstrom, S. F. T., Jones, B. B., & Wilson, R. 1973, A&A, 22, 161

Bruner, E. C., & McWhirter, R. W. P. 1979, ApJ, 231, 557

Bruner, E. C., Parker, R. W., Chipman, E., & Stevens, R. 1973, ApJ, 182, L33

Cheng, C. C., Doschek, G. A., & Feldman, U. 1979, ApJ, 227, 1037

Chae, J., Schühle, U., & Lemaire, P. 1998, ApJ, 505, 957

Chae, J., Yun, H. S., & Poland, A. I. 1998, ApJS, 114, 151

Dere, K. P., Bartoe, J. -D. F., Brueckner, G. E., Cook, J. W., & Socker, D. G. 1987, Solar Physics, 114, 223

Dere, K. P., Landi, E., Mason, H. E., Monsignori Fossi, B. C., & Young, P. R. 1997, A&AS, 125, 149

Dere, K. P., & Mason, H. E. 1993, Solar Physics, 144, 217

Doschek, G. A., Feldman, U., & Cohen, L. 1977, ApJS, 33, 10

Doschek, G. A., Feldman, U., van Hoosier, M. E., & Bartoe,J. -D. F. 1976, ApJS, 31, 417

Doyle, J. G., Banerjee, D., & Perez, M. E. 1998, Solar Physics, 181, 91

Doyle, J. G., O'Shea, E., Erdélyi, R., Dere, K. P., Socker, D. G., & Keenan, F. P. 1997, Solar Physics, 173, 243

Dwivedi, B. N. 1994, Space Sci. Rev. 65, 289

Erdélyi, R., Doyle, J. G., Perez, M. E., & Wilhelm, K. 1998, A&A, 337, 287

Feldman, U., Doschek, G. A., & Patterson, N. P. 1976, ApJ, 209, 270

Feldman, U., Doschek, G. A., & Tousey, R. 1975, ApJ, 202, L147

Hassler, D. M., Rottman, G. J., Shoub, E. C., & Holtzer, T. E. 1990, ApJ, 348, L77

Hollandt, J., Schühle, U., Paustian, W., Curdt, W., Kühne, M. 1996, Appl. Opt., Vol. 35, No.25

Kjeldseth-Moe, O., & Nicolas, K. R. 1977, ApJ, 211, 579

Landi, E., Landini, M., Dere, K. P., Young, P. R., & Mason, H. E. 1999, A& AS, 135, 339

Lemaire, P. et al. 1997, Solar Physics, 170, 105

Mariska, J. T., Feldman, U., & Doschek, G. A. 1978, ApJ,226, 698

Mariska, J. T., Feldman, U., & Doschek, G. A. 1979, A&A, 73, 361

Mariska, J. T., & Withbroe, G. L. 1975, Solar Physics, 44, 55

McClements, K. G., Harrison, R. A., & Alexander, D. 1991, Solar Physics, 131, 41

Moran, T. 1998, in private communication

Nicolas, K. R., Brueckner, G. E., Tousey, R., Tripp, D. A., White, O. R., & Athay, R. G. 1977, Solar Physics, 55, 305

Peter, H. 1999, ApJ, 516, 490

Roussel-Dupré, R., Francis, M. H., & Billings, D. E. 1979, MNRAS, 187, 9

Seely, J. F., Feldman, U., Schühle, U., Wilhelm, K., Curdt, W., Lemaire, P. 1997, ApJ, 484, L87

Shine, R. A., Roussel-Dupree, D., Bruner Jr., E. C., Chipman, E. G., Lites, B. W., & Rottman, G. J. 1976, ApJ, 210, L107

Tu, C. -Y., Marsch, E., Wilhelm, K., & Curdt, W. 1998, ApJ, 503, 475

Vernazza, J. E., Avrett, E. H., & Loeser, R. 1981, ApJS, 45, 635

Vial, J. C., Lemaire, P., Artzner, G., & Gouttebrose, P. 1980, Solar Physics, 68, 187

Warren, H. P., Mariska, J. T., Wilhelm, K., & Lemaire, P. 1997, ApJ, 484, L91

Wilhelm, K., Marsch, E., Dwivedi, B. N., Hassler, D. M., Lemaire, P., Gabriel, A. H., & Huber, M.C.E. 1998, ApJ, 500, 1023

Wilhelm, K. et al. 1995, Solar Physics, 162, 189

Wilhelm, K. et al. 1997a, Solar Physics, 170, 75

Wilhelm, K., Lemaire, P., Feldman, U., Hollandt, J., Schühle, U., & Curdt, W. 1997b, Appl. Opt., Vol.36, No.25

Withbroe, G. L., & Mariska, J. T. 1976, Solar Physics, 48, 21